EmbodiedDiffusion: End-to-End Traversability-Guided Visual Diffusion for Heterogeneous Robot Navigation

Iana Zhura, Sausar Karaf, Faryal Batool, Nipun Dhananjaya Weerakkodi Mudalige, Valerii Serpiva, Ali Alridha Abdulkarim, Aleksey Fedoseev, Didar Seyidov, Hajira Amjad, Dzmitry Tsetserukou

arXiv:2512.02851v4 [cs.RO] 16 Jul 2026

***Abstract*—Visual traversability estimation is central to autonomous navigation, yet most approaches either rely on prompt-driven Vision-Language Model (VLM) or decouple traversability from trajectory planning, requiring separate planners with heavy mapping, manual tuning, and extended deployment time. We propose *EmbodiedDiffusion*, a diffusion-based framework that simultaneously predicts traversability maps and generates feasible trajectories from RGB images using planner-free synthetic supervision and embodiment conditioning for cross-platform transfer. The framework distills category-level traversability semantics from a VLM teacher into a lightweight student model during training, enabling prompt-free, real-time inference at deployment. A modular FiLM-based conditioning mechanism isolates embodiment-specific reasoning into a compact trainable subset of the network, allowing rapid adaptation to new robot platforms without retraining the visual backbone or the trajectory diffusion model. Across indoor environments with quadruped and aerial robots, *EmbodiedDiffusion* achieves 80–100% navigation success in the full-data regime with real-time inference (90 ms) and adapts to new platforms using only ∼10 min of visual data collection, demonstrating scalable, unified traversability reasoning and trajectory generation for heterogeneous robots.**

I. Introduction

Indoor navigation enables warehouse automation, inspection, and search-and-rescue [1], [2], requiring simultaneous traversability reasoning and trajectory generation in cluttered environments where small errors cause failure.

Classical geometric pipelines rely on explicit metric maps and careful tuning, making them brittle under occlusions and irregular geometry. Self-supervised visual traversability methods [3], [4] reduce map dependence but remain tightly coupled to the sensing modality and embodiment that generated the supervision, requiring retraining for each new platform. VLM offers greater flexibility but requires per-scene, per-embodiment prompt tuning at deployment, a significant overhead in practice [5], [6]. Critically, most existing learned navigation approaches either memorize expert trajectory datasets or depend on planner-generated ground truth, limiting generalization to distributions not seen during training [7], [8].

We propose *EmbodiedDiffusion*, a diffusion-based framework that simultaneously predicts traversability maps and generates feasible trajectories from a single RGB image, trained without expert demonstrations using planner-free synthetic supervision. VLM knowledge is distilled offline into a compact student model that performs prompt-free at inference, eliminating per-scene tuning while preserving the semantic richness of VLM. A modular FiLM-based embodiment conditioning mechanism isolates platform-specific reasoning into a lightweight trainable subset, keeping the visual backbone and trajectory diffusion model frozen to enable rapid cross-platform adaptation from only 10 min of data.

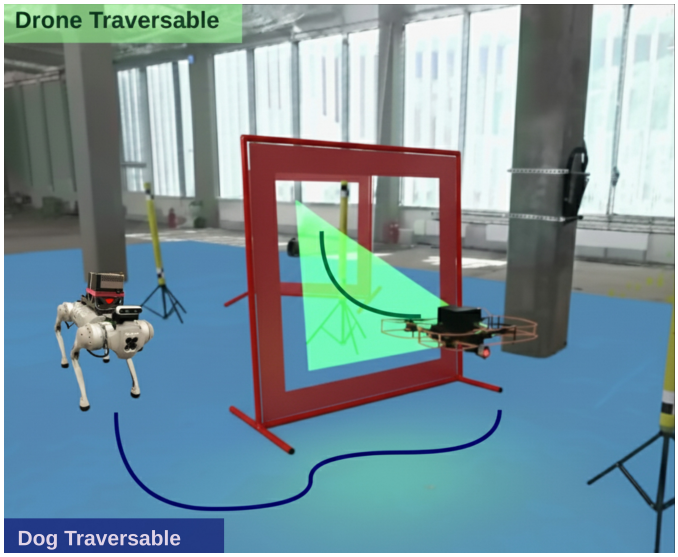


Fig. 1: Cross-embodiment traversability and trajectory generation from a shared visual backbone. A single network conditioned on the robot state vector via FiLM produces embodiment-specific behavior from the same RGB scene: the quadruped (blue) routes around the gate while the aerial robot (green) flies through it, with only a lightweight trainable subset adapted per platform.

Our main contributions can thus be summarized as follows:

- **Unified traversability and trajectory generation from RGB images.** A single diffusion model that simultaneously predicts traversability and generates feasible trajectories from RGB images, without expert demonstrations or mapping. VLM supervision is distilled offline into a compact prompt-free student model running at 90 ms on edge hardware.
- **Planner-free synthetic supervision with traversability regularization.** Trajectories are learned from geometrically generated heatmaps, where $\mathcal{L}_{\text{trav}}$ concentrates the probability mass in visually safe regions. Learning the trajectory distribution rather than memorizing specific paths yields stronger generalization and outperforms expert-supervised baselines in obstacle clearance.
- **Modular embodiment-conditioned adaptation.** A FiLM-based mechanism that freezes the DINOv2 backbone and diffusion UNet while retraining only the lightweight ViT adapter, state encoder, and decoder, en-

The authors are with the Intelligent Space Robotics Laboratory, Center for Digital Engineering, Skolkovo Institute of Science and Technology. {iana.zhura, sausar.karaf, faryal.batool, nipun.weerakkodi, valerii.serpiva, ali.abdulkarim, aleksey.fedoseev, didar.seyidov, hajira.amjad, d.tsetserukou}@skoltech.ru

abling new platform adaptation from 10 min of visual data.

- **Heterogeneous real-world and simulation-based validation.** We provide a complete ROS2 navigation framework validated on a quadruped (Unitree Go1) and a custom aerial platform, alongside a Unity simulation environment developed for safe UAV testing, achieving 80–100% success in the full-data regime at 90 ms inference. Code, dataset, and simulation environments will be released upon acceptance.

II. Related Work

A. Traversability Estimation from Vision

Self-supervised traversability estimation derives supervision from a robot's own interactions and regresses it from visual perception, using RGB [9], [10], depth, or LiDAR inputs [11]–[13]. While some recent work has explored fast adaptation using pre-trained visual features for traversability prediction [3], these methods focus solely on traversability without trajectory generation. More broadly, self-supervised approaches require extensive physical interaction and are tightly coupled to the embodiment and sensing configuration that generated the supervision, limiting transfer to new platforms and environments [14], [15].

VLM approaches [5], [16] reduce this burden but require per-deployment prompt tuning for each embodiment and scene, which is a prohibitive cost in practice. SALON [17] automates refinement through online exploration but still incurs deployment-time overhead.

Existing methods either require physical interaction and deployment-time prompt engineering, or decouple traversability from planning, incurring mapping and tuning overhead. We address this by distilling embodiment-specific traversability cues from a VLM offline into a lightweight student, enabling prompt-free, unified traversability-trajectory generation at deployment.

B. Diffusion-Based Motion Planning

Diffusion models have recently been applied to motion generation, including quadruped pose diffusion (DiPPeST) [18], goal-conditioned exploration (NoMaD) [19], cost-aware trajectory generation (MPD) [20], and image-based navigation (VENTURA [21], NaviDiffusor [22]). While effective, these methods require expert demonstrations or planner-generated ground truth, rely on precomputed costmaps or external traversability estimates, and treat traversability and trajectory generation as separate processes. For aerial robots specifically, Artificial Potential Field (APF) based indoor planners are computationally expensive and difficult to tune when operating directly on dense 3D point clouds, while GPS-dependent outdoor methods fail in GPS-denied environments [23]. Critically, no existing diffusion-based planner unifies navigation across fundamentally different embodiments such as ground and aerial robots. In contrast, we simultaneously learn traversability and trajectory generation from vision using planner-free synthetic supervision, without curated datasets or geometric optimization at deployment.

III. Technical Approach

A. Network Architecture

Our framework couples two components: (1) a traversability student model that distills embodiment-specific scene understanding from a VLM teacher model, and (2) a diffusion-based trajectory generator conditioned on the predicted traversability, the robot state vector, and supervised by synthetic trajectories.

1) Synthetic Trajectory Supervision: To supervise trajectory diffusion without expert demonstrations, we generate synthetic trajectory heatmaps using a simple geometric procedure. For each training image, we sample a start point s near the image bottom and a goal point g in a high-traversability region identified by the VLM teacher model. We generate smooth paths by sampling $K{=}5$ intermediate waypoints along $s{\to}g$, applying random perpendicular perturbations sampled from $\mathcal{N}(0, \sigma^2)$, smoothing via cubic splines, and rasterizing as thin traces on a $64{\times}64$ grid.

These heatmaps provide soft supervision that encodes connectivity and directionality without requiring geometric optimality. This is deliberate: because synthetic paths are heuristically generated rather than expert-optimal, the model learns the underlying distribution of feasible trajectories rather than memorizing specific paths. Geometric path quality is further encouraged through path length and smoothness regularization, and start-goal consistency is enforced via an explicit anchoring loss, both described in Section III-B.

2) Traversability Teacher and Student Model: Traversability supervision comes from the AnyTraverse VLM [5], which provides platform-specific traversability maps as training targets and trajectory conditioning signals.

Distillation is a deliberate design choice: the VLM teacher model is too large and prompt-dependent for real-time onboard inference. By extracting its traversability knowledge offline once per embodiment type, we obtain a compact student model that runs at 90 ms on edge hardware without any prompting at deployment.

The traversability student model uses a frozen DINOv2 ViT [24] with a lightweight adapter [25]. Robot state $s_t = [x, y, z, \text{roll}, \text{pitch}, \text{yaw}] \in \mathbb{R}^6$ encodes camera pose, enabling embodiment-specific predictions via FiLM conditioning on visual features. This captures platform-specific viewpoints and reachable regions without modeling full dynamics.

The robot state vector $s_t \in \mathbb{R}^6$ is encoded by an MLP to produce FiLM (Feature-wise Linear Modulation [26]) parameters $(\gamma_t, \beta_t) \in \mathbb{R}^C$, which modulate the visual feature map $\mathbf{F} \in \mathbb{R}^{C \times H \times W}$ via a channel-wise affine transformation:

$$\tilde{\mathbf{F}} = \mathbf{F} \odot (1 + \gamma_t) + \beta_t, \tag{1}$$

where $\odot$ is the element-wise (Hadamard) product, C is the number of feature channels, and $H \times W$ is the spatial resolution. This conditioning allows the same visual scene to yield embodiment-consistent traversability predictions. A compact convolutional decoder produces a dense $64{\times}64$ traversability map $\hat{T}_t$.

3) Diffusion-Based Trajectory Policy: Trajectory generation is performed using a conditional UNet diffusion model. At denoising step t, the network predicts the injected noise

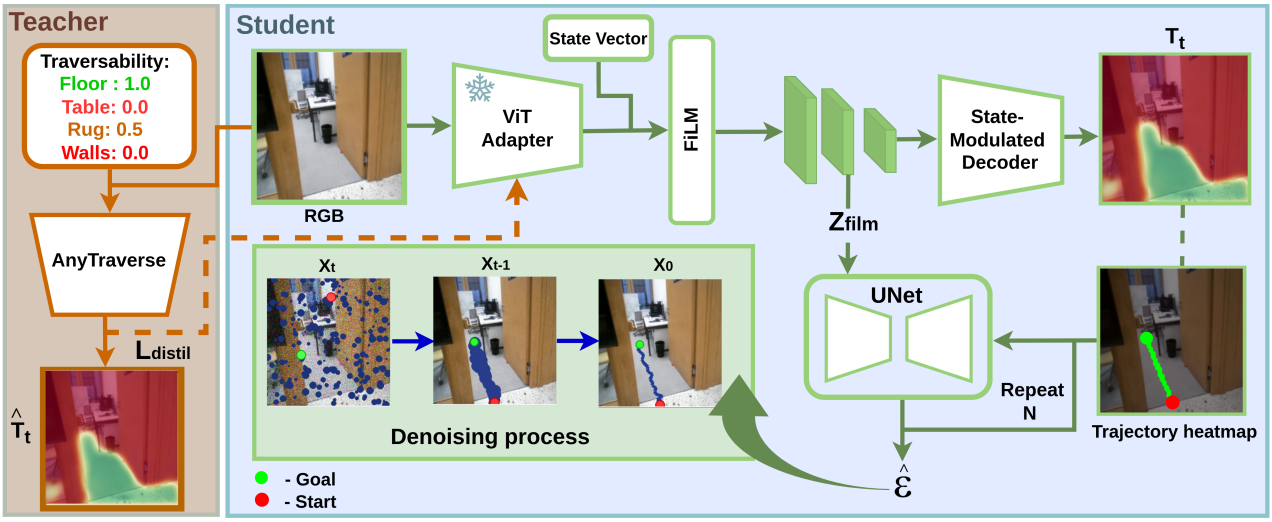


Fig. 2: Two-component framework. *Teacher model* (left): AnyTraverse [5] produces a dense traversability map $\hat{T}_t$ from the RGB image and embodiment-specific prompts (e.g., Floor: 1.0, Walls: 0.0), supervising the student model via $\mathcal{L}_{\text{distil}}$. *Student model* (right): a frozen visual encoder is modulated by the robot state vector through FiLM conditioning [26], producing embodiment tokens Z_{film} and a predicted traversability map $\hat{T}_t$ via the State-Modulated Decoder. $\mathbf{Z}_{\text{film}}$ additionally conditions the diffusion UNet via cross-attention. The UNet denoises a trajectory sample $x_t \to x_0$ over N=20 steps, conditioned on trajectory heatmap overlay and predicted traversability map $\hat{T}_t$. The Teacher model runs offline during training only; at inference the Student model runs prompt-free at 90 ms.

$\hat{\varepsilon}_t$ conditioned on the noisy trajectory sample x_t, the start-goal map S_g, the predicted traversability $\hat{T}_t$, and embodiment tokens Z_{film} obtained from the same FiLM-conditioned state encoding used in the traversability model:

$$\hat{\varepsilon}_t = f_\theta([x_t, S_g, \hat{T}_t], t, Z_{\text{film}}). \tag{2}$$

Spatial conditioning ensures that denoising remains aligned with traversable regions, while token-level conditioning injects embodiment priors through cross-attention.

The model is trained using the standard DDPM (Denoising Diffusion Probabilistic Models [27]) noise prediction objective which is defined as:

$$\mathcal{L}_{\text{DDPM}} = \|\hat{\varepsilon}_t - \varepsilon\|_2^2, \quad \varepsilon \sim \mathcal{N}(0, I). \tag{3}$$

Trajectories are generated at inference time by iteratively denoising from $x_T \sim \mathcal{N}(0, I)$ using a cosine noise schedule. The final output x_0 is a clean trajectory heatmap that is simultaneously consistent with scene geometry, traversability, and robot embodiment.

B. Learning Objectives

The training objective is designed to encourage four complementary properties: (i) globally coherent trajectory structure via diffusion-based denoising, (ii) alignment of predicted trajectories with visually traversable regions, (iii) embodiment-consistent interpretation of traversability through distillation, and (iv) geometric path quality via length and smoothness regularization.

Let the predicted trajectory heatmap be $x_0 \in [0,1]^{H\times W}$, the noisy diffusion state at timestep t be x_t, and the predicted traversability map be $\hat{T}$.

1) Diffusion Objective: Trajectory generation is trained using the standard DDPM noise prediction objective. Given injected noise $\varepsilon \sim \mathcal{N}(0, I)$, the model predicts $\hat{\varepsilon}_t$ and minimizes:

$$\mathcal{L}_{\text{noise}} = \|\hat{\varepsilon}_t - \varepsilon\|_2^2. \tag{4}$$

This objective enables the model to learn a multimodal distribution over feasible trajectory structures conditioned on visual and embodiment cues.

2) Traversability Alignment: To bias trajectories toward safe regions, we define a spatial probability distribution over the predicted trajectory heatmap using a global softmax:

$$p(u, v) = \frac{\exp(x_0(u, v)/\tau)}{\sum_{i,j} \exp(x_0(i, j)/\tau)}, \tag{5}$$

where (u, v) denote pixel coordinates and $\tau > 0$ is a temperature parameter.

The expected traversability under this distribution is:

$$\mathbb{E}_p[\hat{T}] = \sum_{u,v} p(u, v)\, \hat{T}(u, v), \tag{6}$$

and we minimize:

$$\mathcal{L}_{\text{trav}} = 1 - \mathbb{E}_p[\hat{T}], \tag{7}$$

which encourages probability mass to concentrate in visually traversable regions without enforcing hard geometric constraints.

3) Traversability Distillation: The traversability student model is trained via ℓ_1 distillation from the teacher model prediction T:

$$\mathcal{L}_{\text{distil}} = \frac{1}{HW} \sum_{u,v} \left| \hat{T}(u, v) - T(u, v) \right|, \tag{8}$$

where $H \times W$ denotes the spatial resolution of the heatmap (64×64 in all experiments).

4) Geometric Path Regularization: To improve geometric consistency, we apply lightweight trajectory regularization during training. Let $\{p_i\}_{i=1}^{K}$ denote the ordered waypoints extracted from the predicted trajectory heatmaps via differ-

entiable weighted centroid estimation. The geometric regularization loss is defined as:

$$\mathcal{L}_g = \sum_{i=1}^{K-1} \|p_{i+1} - p_i\|_2 \; + \; \alpha \sum_{i=2}^{K-1} \|p_{i+1} - 2p_i + p_{i-1}\|_2^2, \quad (9)$$

where the first term penalizes trajectory path length and the second encourages smoothness via the discrete second-order derivative. The weighting coefficient α controls the smoothness strength, and is empirically set to $\alpha = 0.1$ in all experiments based on validation performance.

5) Final Objective: The full training objective is given by:

$$\mathcal{L} = \mathcal{L}_{\text{noise}} + \lambda_{\text{trav}}\mathcal{L}_{\text{trav}} + \lambda_{\text{distil}}\mathcal{L}_{\text{distil}} + \lambda_{\text{g}}\mathcal{L}_{\text{g}}, \quad (10)$$

where λ_{trav}, λ_{distil}, and λ_{g} are the fixed scalar weights used in all experiments.

C. Scene Generalization

Traversability prompts are formulated at the category level rather than the scene level: broad surface categories for ground robots (*floor*, *walls*, and *rugs*) and embodiment-specific affordances for aerial robots (*narrow gaps*, *low ceilings*). Encoding traversability categories rather than specific visual instances allows the teacher model to transfer naturally to unseen scenes sharing the same semantic structure, as confirmed by the cross-scene experiments in Section IV-G4.

D. Modular Embodiment Adaptation

The DINOv2 backbone and diffusion UNet are frozen across embodiments; only the ViT adapter, FiLM modulation, state encoder, and decoder are retrained per platform, enabling efficient adaptation from as few as 4,000 RGB images in 10 min. Crucially, training data from multiple embodiments can be mixed within a single training run: the FiLM mechanism conditions visual features on the robot state vector, making each embodiment's predictions distinguishable from one another without requiring separate models or isolated training sets. This coupling between body-specific state and visual features ensures that the shared backbone learns platform-agnostic scene representations while the lightweight trainable subset captures the physical constraints of each robot, as reported in Section IV-G2.

IV. Experiments and Results

A. UAV Simulation

For safety, we developed a Unity-based UAV simulation (Fig. 3) following Flightmare [28], decoupling visual rendering from dynamics. The ROS-based controller sends state to Unity, which provides RGB, depth, and point cloud data. Our diffusion pipeline generates a path mask from RGB, projected onto the point cloud to extract 3D waypoints. The same extraction method is used in real-world deployment.

B. Dataset Generation

We collected 4,000 RGB images per embodiment using an Intel RealSense D435i on a Unitree Go1 and a custom UAV. Robot state vectors encoding camera pose are extracted from visual odometry. For each frame, synthetic trajectories are generated automatically: starts sampled near the image bottom, goals in distant high-traversability regions. Training on 8,000 samples on an NVIDIA RTX 4090 requires 1.5 hours and 6 GB memory.

C. Metrics

We evaluate feasibility and safety against diffusion baseline, as our contribution is visual-to-motion inference rather than trajectory optimization. Metrics include success rate, clearance (average obstacle distance), traversability cost (normalized teacher-derived cost), and Safe_{min}, Safe_{max} (fraction of points with > 0.2 m clearance).

D. Ablation Studies

All ablation studies are performed on a held-out validation split with unseen environments, and the best configuration is subsequently used for all real-robot and simulation deployment, ensuring no test-set leakage.

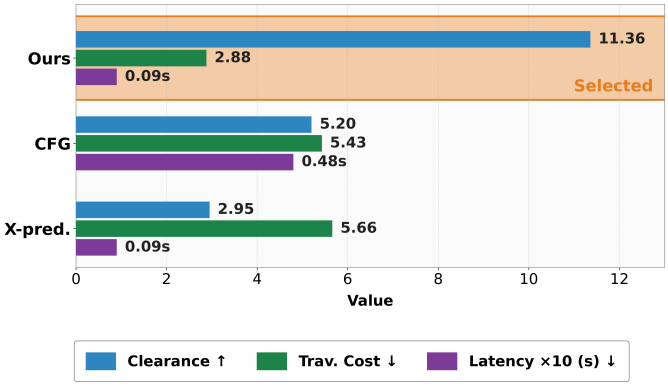


Fig. 4: Ablation of diffusion design choices. *Ours* combines conditional traversability guidance with ε-prediction (noise prediction). *CFG* degrades clearance by 54% and slows inference 5×; *X-pred.* (sample prediction, in which the clean sample x_0 is predicted directly) degrades clearance by 74% due to overfitting on imperfect synthetic supervision.

1) Influence of Different Components: As shown in Table I, all components contribute positively to trajectory quality. Removing traversability input reduces clearance by 26% and increases cost by 19%, confirming its role in safe navigation. Most critically, disabling conditional embedding causes the largest performance drop (clearance falls 49%, from 11.36 to 5.83), demonstrating that embodiment-aware conditioning is essential for generating platform-specific feasible trajectories.

TABLE I: Ablation: Network Components.

Variant	Clear. ↑	Cost ↓	Saf._{min} ↑	Saf._{max} ↑
Full model	**11.36**	**2.88**	**0.96**	**0.98**
No trav. input	8.37	3.42	0.93	0.98
No s_g input	11.26	3.37	0.95	0.98
No cond. emb.	5.83	5.34	0.90	0.97

2) Diffusion Policy Design: We evaluate two critical design decisions: guidance strategy and generative formulation. As shown in Fig. 4, our approach substantially outperforms alternatives. Conditional traversability guidance achieves 11.36 clearance and 2.88 cost, while classifier-free guidance (CFG)

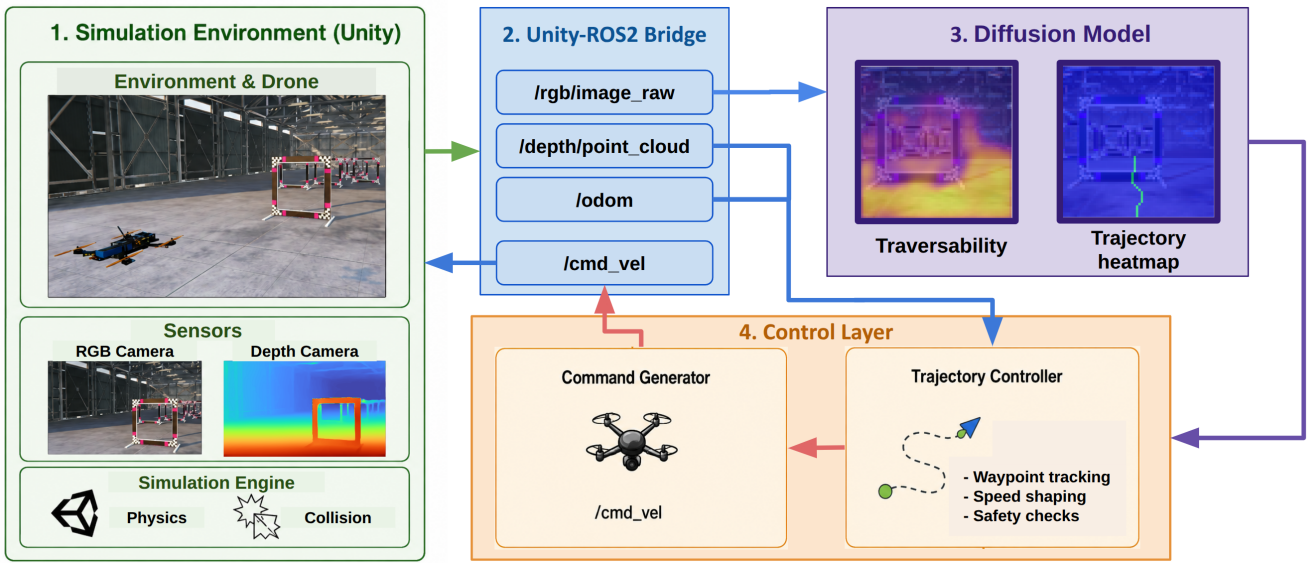


Fig. 3: UAV simulation architecture. A closed-loop pipeline of four stages: (1) Unity renders the scene and drone with physics and collision, providing RGB and depth streams; (2) a Unity–ROS2 bridge exchanges sensor data and velocity commands; (3) the diffusion model predicts a traversability map and trajectory heatmap from RGB; and (4) the control layer extracts 3D waypoints from the heatmap and depth, tracking them before issuing velocity commands back to the simulator. Decoupling rendering from dynamics enables safe UAV testing, with the same extraction used in real-world deployment.

degrades to 5.20 clearance and 5.43 cost with 5× slower inference (0.48 s vs. 90 ms). CFG's double forward pass and signal amplification, designed for weak text conditioning, prove detrimental when strong multi-modal conditioning (traversability, goal, embodiment) is already present. For generative formulations, we compare ε-prediction (noise prediction) against sample prediction (X-pred.), which directly predicts the clean trajectory x_0. The former maintains 11.36 clearance, while the latter collapses to 2.95 (74% degradation). Since our synthetic trajectories are heuristic rather than expert-optimal, ε-prediction learns the underlying distribution and deviates from imperfect supervision, outperforming the direct MSE fitting of sample prediction.

3) Denoising Process: Figure 5 shows clearance peaks at 20 steps (11.36 pixels, 90 ms), balancing quality and speed. Single-step inference yields poor performance (2.75 clearance), while 100 steps provide marginal gains at 4× latency cost.

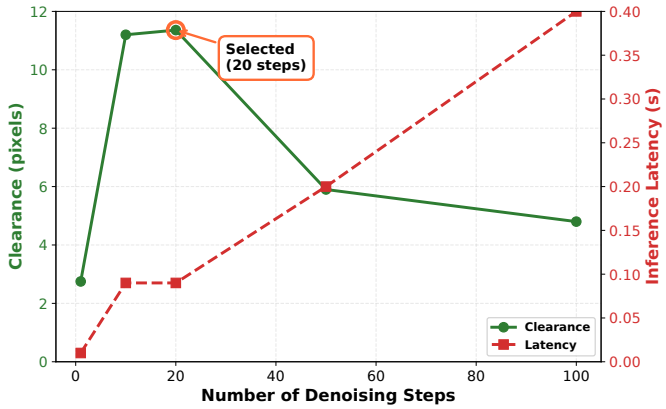


Fig. 5: Denoising step analysis. We select 20 steps (highlighted) as it achieves peak clearance (11.36) with real-time latency (90 ms).

E. Baselines

As no existing method simultaneously performs traversability estimation and diffusion-based trajectory generation across heterogeneous embodiments, we establish two baselines for controlled comparison. First, we adapt DTG [29] by retraining with front-view RGB and manually annotated expert trajectories (11,500 aerial, 8,000 multi-embodiment), isolating the effect of our planner-free synthetic supervision against dense expert demonstrations. Second, we implement Potential Fields + VLM, which combines the AnyTraverse teacher model for traversability estimation with classical gradient-based trajectory planning, allowing us to compare learned diffusion against gradient-based optimization on identical traversability inputs.

F. Simulation Deployment

At deployment, the trajectory heatmap is projected onto the corresponding depth point cloud to extract 3D waypoints, which are then converted to robot base frame coordinates and sent to the controller for trajectory tracking.

We validate the approach in simulation across five diverse scenarios with varying obstacle densities. As shown in Table III, the model achieves 80% success rate with 0.33 m average clearance despite being trained exclusively on real-world RGB data. The performance gap compared to real deployment (80% vs. 100% in simpler scenarios) stems from higher noise and artifacts in simulated depth sensors versus real RealSense data, suggesting future work could predict depth directly along candidate trajectories from RGB input.

G. Real-World Deployment

We evaluate on two platforms. The UAV is a custom 8-inch quadrotor running ArduPilot with MAVROS high-level control, onboard state estimation via OpenVINS [30] with a RealSense T265, and off-board trajectory generation. The

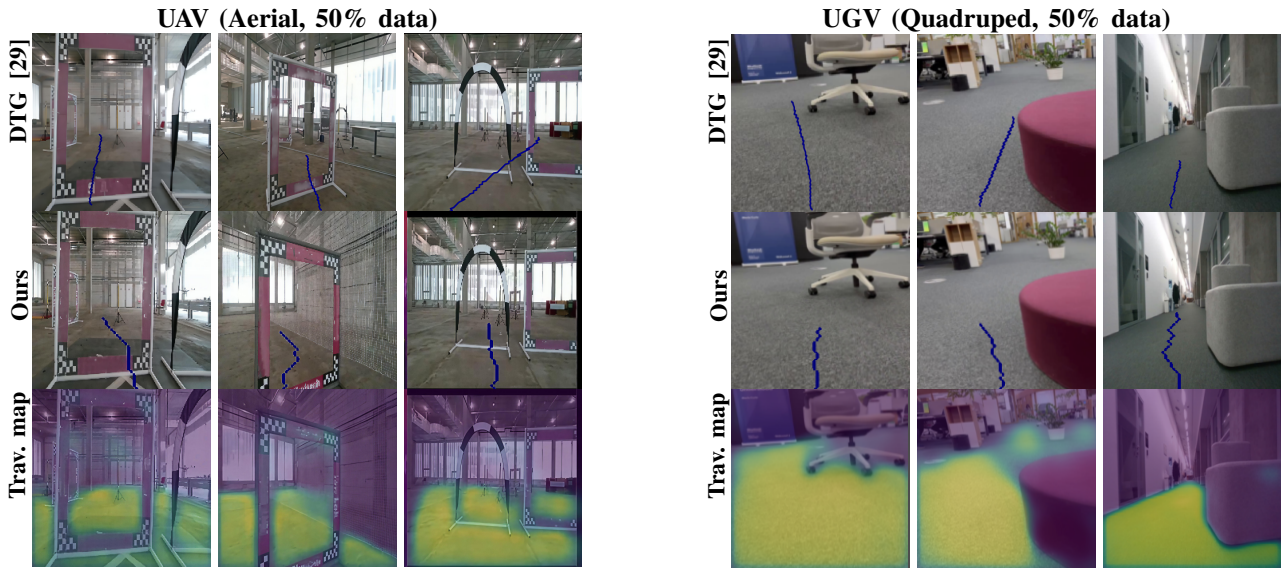


Fig. 6: Qualitative comparison between DTG [29] baseline and *EmbodiedDiffusion* on aerial and quadruped platforms, with our predicted traversability map shown in the bottom row. A revealing case appears in the UAV columns containing both a black-and-white and a purple gate: DTG consistently selects the same purple gate across scenes because it was trained to imitate expertly-labeled ground-truth trajectories that always passed through that specific gate. *EmbodiedDiffusion*, which learns the distribution of feasible paths via traversability regularization rather than memorizing specific trajectories, recognizes any narrow opening as traversable and selects gates based on the predicted traversability map. This directly demonstrates that distribution-level learning generalizes beyond the specific examples seen during training.

ground robot is a Unitree Go1 quadruped with a front-mounted RealSense D435i, running inference and control onboard on an NVIDIA Jetson Orin AGX for velocity-based tracking via the robot SDK. Notably, the pipeline requires neither global localization nor pre-built maps: trajectories are egocentric and regenerated each inference cycle in the robot's current camera frame.

Trajectory projection and safety. At each inference cycle, the diffusion model jointly predicts trajectory heatmaps and a traversability map, where the traversability prediction guides the denoising process toward safe and navigable regions. The traversability map is additionally used to estimate the local proportion of traversable area around the robot, helping avoid cornering and dead-end situations.

Near-field trajectory predictions are typically geometrically consistent, while uncertainty increases for longer-range predictions due to ambiguity in monocular RGB depth perception. To prevent this uncertainty from propagating into execution, predicted trajectory heatmaps are projected onto the RealSense depth point cloud to recover 3D waypoints in the robot base frame. Because the diffusion model produces only a small set of trajectory candidates, a localized Artificial Potential Field (APF) cost is evaluated only on this candidate set rather than over the full point cloud. Each candidate is scored using goal progress and obstacle clearance, and the best-scoring trajectory is executed. This lightweight selection mechanism prevents long-range depth ambiguity from propagating into the executed 3D path. The 90 ms inference cycle further enables continuous replanning, allowing transient errors to be corrected in subsequent planning steps.

1) Comparison with Baselines: Figure 6 shows our method generates safe trajectories comparable to the supervised baseline without ground-truth annotations, while maintaining better cross-embodiment consistency through traversability-guided diffusion.

Table II reveals platform-dependent baseline performance: Potential Fields succeeds on UGV (100%) but fails on UAV (50%), while DTG achieves 60–75% success with expert supervision. Under this matched-comparison protocol, our method achieves 89% success on the UAV and 100% on the UGV at the fastest inference (90 ms), outperforming DTG (60–75%) on identical platforms without any expert supervision.

A particularly informative qualitative observation supports the distribution-learning argument from Section III-A1. In the UAV scenes containing two visually distinct gates (black-and-white and purple), DTG consistently selects the purple gate across all evaluations because its training trajectories — manually annotated and expertly executed — always passed through that specific gate. The model effectively memorizes the gate identity rather than learning the underlying concept of traversable openings. In contrast, *EmbodiedDiffusion* selects gates based on the predicted traversability map, recognizing either gate as a valid traversable passage. This behavioral difference, visible in Fig. 6, illustrates the practical generalization benefit of distribution learning over imitation: our method does not need to encounter every specific obstacle configuration during training to handle it correctly at deployment.

In addition to the baseline comparison, our real-world experiments evaluate the proposed framework across heterogeneous platforms (a quadruped and an aerial robot) along three deployment-oriented dimensions:

- *Embodiment conditioning*: verifying that generated trajectories are physically valid for each platform.
- *Data efficiency*: assessing performance under reduced embodiment-specific training data.
- *Cross-scene generalization*: evaluating transfer to unseen

TABLE II: Baseline Comparison Across Heterogeneous Platforms.

Method	Time, ms↓	Clear.↑	$\text{Safe}_{\min}$ ↑	$\text{Safe}_{\max}$ ↑	Success↑
UAV (Aerial Robot)					
DTG	240	4.85	0.26	0.69	60%
PF + VLM	600	3.56	0.37	0.29	50%
Ours	**90**	**8.75**	**0.50**	**0.80**	**89%**
UGV (Quadruped Robot)					
DTG	240	8.67	0.55	0.83	75%
PF + VLM	160	10.31	0.97	0.90	100%
Ours	**90**	**10.45**	**0.72**	**0.85**	**100%**

indoor environments.

For each deployment scenario, we report success rate and minimum obstacle clearance (from RealSense point clouds). Success requires reaching the goal without collision or intervention. Each scenario comprises five trials with averaged metrics.

2) Embodiment Conditioning: Table III shows successful cross-platform deployment: quadrupeds achieve 0.41–1.19 m clearance (ground-based spatial freedom) while aerial robots maintain 0.31–0.45 m in tighter corridors. Both achieve 67–100% success, demonstrating that embodiment conditioning captures platform-specific constraints without separate models.

The body-specific state vector, combined with visually similar training environments shared across platforms, allows the model to distinguish between embodiments and generate platform-appropriate behaviors. This is most evident in the quadruped trajectories: rather than attempting to navigate through narrow openings as an aerial robot would, the quadruped consistently plans routes around tight areas, reflecting its ground-based spatial constraints and wider physical footprint. This platform-specific behavior emerges purely from the FiLM-modulated state conditioning without any explicit rule encoding or separate model per platform.

3) Data Efficiency: We evaluate the quadruped across three training data regimes (100%, 50%, 30%). As shown in Table III, the model maintains 100% navigation success under both full and half-data settings, achieving obstacle clearances of 1.19 m and 0.41 m, respectively. Performance degrades at 30% training data (67% success, 0.56 m clearance), suggesting an effective generalization threshold near 50% of the original dataset. These results indicate that the distilled VLM priors provide strong semantic and geometric regularization, enabling robust traversability prediction even under substantially reduced supervision.

4) Cross-Scene Generalization: We evaluate the aerial robot on three unseen scenarios: single gate, gate with novel obstacle, and sequential gates (2G). Across all scenarios, the gates were further varied by occluding them with different types of objects placed both in front of and behind the gate, testing whether the framework can correctly identify the traversable opening despite changes in surrounding visual context. The drone achieves 100% success (0.45 m and 0.40 m clearance) on the single-gate and gate-with-obstacle scenarios, and drops to 67% (0.31 m clearance) on the sequential-gate (2G) scenario due to tighter spatial constraints. Robustness to foreground and background occlusion further supports the generalization argument from Section III-C: the framework recognizes traversability based on the geometry of the opening rather than memorizing specific scene layouts.

TABLE III: Real-world deployment results across three settings: UGV data efficiency (100%, 50%, 30%), UAV cross-scene generalization (G, 2G, GO), and UAV sim-to-real transfer. Highlighted rows indicate the best-performing configuration in each setting.

Experiment	Setting	Success ↑	Clearance (m) ↑
UGV — data efficiency (quadruped robot)			
UGV	100% data	**100%**	**1.19**
UGV	50% data	**100%**	0.41
UGV	30% data	67%	0.56
UAV — cross-scene generalization (aerial robot)			
UAV	Single gate (G)	**100%**	0.45
UAV	Sequential gates (2G)	67%	0.31
UAV	Gate + obstacle (GO)	**100%**	0.40
UAV — simulation-to-real transfer			
UAV Sim	Five sim scenarios	80%	0.33

Failures were defined by clearance below 0.2 m rather than actual collisions, occurring when conservative human intervention was triggered by depth sensor distortion that degraded close-range distance estimation.

V. Limitations and Future Work

A. Limitations

The framework generates trajectory heatmaps in image space, which are projected onto depth point clouds for 3D waypoint extraction. This step introduces sensitivity to depth sensor noise: in simulation, degraded point cloud quality reduced success rate to 80% compared to 100% in real-world conditions, and robustness remains limited in environments with reflective surfaces or sensor occlusion.

B. Future Work

Three directions are identified for future development.

1) BEV Trajectory Diffusion from Temporal RGB: We plan to migrate the trajectory representation from image-space heatmaps to a Bird's Eye View (BEV) representation built from temporal RGB sequences and supervised during training with depth-based BEV maps. Using multi-frame visual cues to recover spatial structure removes the dependence on depth projection, enabling metric-scale planning from monocular RGB alone and improving robustness to sensor noise and occlusion.

2) Semantic-Aware Goal Selection: Unlike most diffusion-based planners, *EmbodiedDiffusion* requires no continuous intermediate goal input, instead selecting the most traversable region as the target. We will extend this with DINOv2 attention maps to autonomously identify semantically meaningful targets such as doorways or docking stations, further reducing supervision without explicit object detection.

3) Online Traversability Refinement: The distilled VLM priors provide strong semantic traversability estimates, allowing the robot to avoid operating purely from sparse online feedback. Instead, the system starts from rich prior world knowledge and can incrementally refine its traversability understanding through onboard observations and physical interaction, similar to how humans adapt prior experience to

new environments. Future work will explore online refinement using onboard sensing modalities such as IMU and proprioceptive feedback, enabling adaptation towards finer body-dynamic constraints and capturing surface properties and physical interactions beyond what RGB observations alone can provide.

VI. Conclusion

We presented *EmbodiedDiffusion*, a unified traversability-guided diffusion framework that simultaneously predicts traversability and generates feasible trajectories directly from RGB observations, enabling embodiment-conditioned navigation without expert demonstrations, explicit geometric maps, or deployment-time prompt engineering. By distilling VLM-based traversability reasoning into a compact diffusion model, the proposed approach learns navigation as a distribution-level traversability problem rather than memorization of expert trajectories.

Experimental results across quadruped and aerial platforms demonstrate that planner-free synthetic supervision is sufficient to achieve robust real-world navigation performance, while lightweight FiLM-based embodiment conditioning enables rapid cross-platform adaptation from only 10 min of data. The proposed end-to-end formulation further improves UAV obstacle clearance by up to 80% over the strongest baseline while operating at $6.7\times$ faster inference.

Together, these results show that a single lightweight onboard model can unify traversability reasoning and trajectory generation across heterogeneous robotic embodiments, providing a scalable foundation for real-time navigation in complex and previously unseen environments.

References

[1] D. A. Gómez-Rosal, M. Bergau, G. K. Fischer, A. Wachaja, J. Grater, M. Odenweller, *et al.*, "A smart robotic system for industrial plant supervision," *IEEE SENSORS*, pp. 1–4, Oct.-Nov. 29-1, 2023.

[2] K. Weerakoon, A. J. Sathyamoorthy, M. Elnoor, and D. Manocha, "Adventr: Autonomous robot navigation in complex outdoor environments," in *Proc. Int. Symposium on Experimental Robotics*, pp. 219–228, Nov. 26-30 2023.

[3] J. Frey, M. Mattamala, N. Chebrolu, C. Cadena, M. Fallon, and M. Hutter, "Fast Traversability Estimation for Wild Visual Navigation," in *Proc. of Robotics: Science and Systems*, 2023.

[4] M. V. Gasparino, A. N. Sivakumar, and G. Chowdhary, "WayFASTER: a Self-Supervised Traversability Prediction for Increased Navigation Awareness," in *Proc. IEEE Int. Conf. on Robotics and Automation (ICRA)*, pp. 8486–8492, May 13-17, 2024.

[5] S. Sahu, A. Singh, K. Nambiar, S. Saripalli, and P. Sujit, "AnyTraverse: An off-road traversability framework with VLM and human operator in the loop," 2025. arXiv:2506.16826.

[6] O. Sautenkov, Y. Yaqoot, A. Lykov, M. A. Mustafa, G. Tadevosyan, A. Akhmetkazy, M. A. Cabrera, M. Martynov, S. Karaf, and D. Tsetserukou, "UAV-VLA: Vision-Language-Action System for Large Scale Aerial Mission Generation," in *Proc. ACM/IEEE Int. Conf. on Human-Robot Interaction (HRI)*, pp. 1588–1592, Mar. 4-6, 2025.

[7] P. von Platen, S. Patil, A. Lozhkov, P. Cuenca, N. Lambert, K. Rasul, *et al.*, "Diffusers: State-of-the-art diffusion models." https://github.com/huggingface/diffusers, 2022.

[8] W. Yu, J. Peng, H. Yang, J. Zhang, Y. Duan, J. Ji, and Y. Zhang, "LDP: A Local Diffusion Planner for Efficient Robot Navigation and Collision Avoidance," in *Proc. IEEE/RSJ Int. Conf. on Intelligent Robots and Systems (IROS)*, pp. 5466–5472, Oct. 14-18, 2024.

[9] S. Jung, J. Lee, X. Meng, B. Boots, and A. Lambert, "V-STRONG: Visual Self-Supervised Traversability Learning for Off-road Navigation," in *Proc. IEEE Int. Conf. on Robotics and Automation (ICRA)*, pp. 1766–1773, May 13-17, 2024.

[10] R. Julian, K. Stone, W. Koch, A. Faust, I. Gilitschenski, and J. P. How, "Badgr: Learning to drive from raw sensor data using self-supervision," in *Proc. Rob.: Sci. and Syst.*, 2020.

[11] E. Chen, C. Ho, M. Maulimov, C. Wang, and S. Scherer, "Learning-on-the-Drive: Self-supervised Adaptive Long-range Perception for High-speed Offroad Driving," in *Proc. IEEE/RSJ Int. Conf. on Intelligent Robots and Systems (IROS)*, pp. 9588–9595, Oct. 14-18, 2024.

[12] H.-S. Yoon, J.-H. Hwang, C. Kim, E. I. Son, S.-W. Yoo, and S.-W. Seo, "Adaptive Robot Traversability Estimation Based on Self-Supervised Online Continual Learning in Unstructured Environments," *IEEE Robotics and Automation Letters*, vol. 9, pp. 4902–4909, April 2024.

[13] F. A. Ruetz, N. Lawrance, E. Hernández, P. V. K. Borges, and T. Peynot, "ForestTrav: 3D LiDAR-Only Forest Traversability Estimation for Autonomous Ground Vehicles," *IEEE Access*, vol. 12, pp. 37192–37206, March 2024.

[14] M. Elnoor, K. Weerakoon, G. Seneviratne, R. Xian, T. Guan, M. K. M Jaffar, V. Rajagopal, and D. Manocha, "VLM-GroNav: Robot Navigation Using Physically Grounded Vision-Language Models in Outdoor Environments," in *Proc. IEEE Int. Conf. on Robotics and Automation (ICRA)*, pp. 2391–2398, May 19-23, 2025.

[15] N. D. W. Mudalige, E. Nazarova, I. Babataev, P. Kopanev, A. Fedoseev, M. A. Cabrera, and D. Tsetserukou, "Dogtouch: Cnn-based recognition of surface textures by quadruped robot with high density tactile sensors," in *Proc. IEEE 95th Vehicular Technology Conference (VTC2022-Spring)*, pp. 1–5, June 19-22, 2022.

[16] D. Song, J. Liang, X. Xiao, and D. Manocha, "VL-TGS: Trajectory Generation and Selection Using Vision Language Models in Mapless Outdoor Environments," *IEEE Robotics and Automation Letters*, vol. 10, pp. 5791–5798, April 2025.

[17] M. Sivaprakasam, S. Triest, C. Ho, S. Aich, J. Lew, I. Adu, W. Wang, and S. Scherer, "SALON: Self-supervised Adaptive Learning for Off-road Navigation," 2024. arXiv:2412.07826.

[18] M. Stamatopoulou, J. Liu, and D. Kanoulas, "DiPPeST: Diffusion-based Path Planner for Synthesizing Trajectories Applied on Quadruped Robots," in *Proc. IEEE Int. Conf. on Intelligent Robots and Systems (IROS)*, pp. 7787–7793, Oct. 14-18, 2024.

[19] A. Sridhar, D. Shah, C. Glossop, and S. Levine, "NoMaD: Goal Masked Diffusion Policies for Navigation and Exploration," in *Proc. IEEE Int. Conf. on Robotics and Automation (ICRA)*, pp. 63–70, May 13-17, 2024.

[20] J. Carvalho, A. T. Le, P. Kicki, D. Koert, and J. Peters, "Motion planning diffusion: Learning and adapting robot motion planning with diffusion models," *IEEE Transactions on Robotics*, vol. 41, pp. 4881–4901, July 2025.

[21] A. Zhang, X. Meng, L. Calliari, D.-K. Kim, S. Omidshafiei, J. Biswas, A. Agha, and A. Shaban, "Ventura: Adapting image diffusion models for unified task conditioned navigation," 2025. arXiv:2510.01388.

[22] Y. Zeng, H. Ren, S. Wang, J. Huang, and H. Cheng, "Navidiffusor: Cost-guided diffusion model for visual navigation," in *Int. Conf. on Robotics and Automation (ICRA)*, pp. 11994–12001, May 19-23, 2025.

[23] X. Wang, Y. R. Tan, W. Leong, S. Huang, R. Teo, and C. Xiang, "GPS Denied IBVS-Based Navigation and Collision Avoidance of UAV Using a Low-Cost RGB Camera," 2025. arxiv:2509.17435.

[24] M. Oquab, T. Darcet, T. Moutakanni, H. Vo, M. Szafraniec, V. Khalidov, *et al.*, "DINOv2: Learning robust visual features without supervision," *Transactions on Machine Learning Research*, Jan. 2024.

[25] D. Bhattacharjee, S. Süsstrunk, and M. Salzmann, "Vision transformer adapters for generalizable multitask learning," in *Proc. IEEE Int. Conf. on Computer Vision (ICCV)*, pp. 18969–18980, 2023.

[26] E. Perez, F. Strub, H. De Vries, V. Dumoulin, and A. Courville, "Film: Visual reasoning with a general conditioning layer," in *Proceedings of the AAAI conference on artificial intelligence*, vol. 32, 2018.

[27] J. Ho, A. Jain, and P. Abbeel, "Denoising diffusion probabilistic models," in *Advances in Neural Information Processing Systems (NeurIPS)*, 2020.

[28] Y. Song, S. Naji, E. Kaufmann, A. Loquercio, and D. Scaramuzza, "Flightmare: A flexible quadrotor simulator," in *Conference on Robot Learning*, 2020.

[29] J. Liang, A. Payandeh, D. Song, X. Xiao, and D. Manocha, "DTG: Diffusion-based Trajectory Generation for Mapless Global Navigation," in *Proc. IEEE/RSJ Int. Conf. on Intelligent Robots and Systems (IROS)*, pp. 5340–5347, Oct. 14-18, 2024.

[30] P. Geneva, K. Eckenhoff, W. Lee, Y. Yang, and G. Huang, "OpenVINS: A Research Platform for Visual-Inertial Estimation," in *Proc. IEEE Int. Conf. on Robotics and Automation (ICRA)*, pp. 4666–4672, May-Aug. 31-31, 2020.